Chiral spin currents and quantum Hall effect in nanotubes

Alex Kleiner
Institute of Theoretical Physics, Chalmers University of Technology and Göteborg University, S-412 96 Göteborg, Sweden
(Received 13 August 2002; revised manuscript received 11 February 2003; published 15 April 2003)

Nanotubes in strong perpendicular magnetic fields are considered and predicted to exhibit chiral spin currents. At a certain filling the current flows only at the sides of the tube, giving rise to the integer quantum Hall effect and magnetoconductance oscillations with a period corresponding to the Aharonov-Bohm flux through the longitudinal cross section of the tube.

DOI: 10.1103/PhysRevB.67.155311 PACS number(s): 72.25.−b, 73.22.−f, 73.43.−f

I. INTRODUCTION

Of the many remarkable properties of nanotubes,[1] a somewhat overlooked feature is the possibility to exert immense gradients of magnetic field on the electrons, by subjecting the tube to a perpendicular homogeneous field; since the electrons on a two-dimensional cylinder are coupled only to the component of the field normal to the surface, the (effective) magnetic field acting on the electron changes sign at the sides of the tube, which may result in very strong gradients. We show here that in sufficiently strong fields [$R>l$, where R is the tube radius and $l=(\hbar/|eB|)^{1/2}$ is the magnetic length] electrons with an opposite direction of propagation are localized in opposite sides of the circumference, forming chiral spin currents, and at a certain energy filling, a Hall quantization.

Spatial control of spin currents was demonstrated previously using a material with a spatially varying g factor.[2] Here, it is the circumferentially varying effective field which is found to generate spin currents along the tube axis.

It was first found numerically in Ref. 3 that a cylindrical two-dimensional electron gas (2DEG) in a perpendicular magnetic field forms Landau-like levels at the top and bottom and chiral states at the sides. Regarding carbon nanotubes, the $\mathbf{k}\cdot\mathbf{p}$ approximation was used to study their magnetoconductance; this approximation, which linearizes the vicinity of the K points of the graphite first Brillouin zone, may be valid at small fields; in strong magnetic fields, however, the K points as well as the graphite first Brillouin zone are ill defined. Even at low fields, the $\mathbf{k}\cdot\mathbf{p}$ theory, did not fare well when compared to experiments.[4,5] A proper account of the specific band structure (i.e., the specific n,m indices of the chiral vector) requires the diagonalization of the magnetic Hamiltonian containing the *complete* carbon-nanotube unit cell, as exposed in Ref. 1. A new class of nanotubes[6,7] forms single inversion layers composed of silicon germanium,[7] indium gallium, and indium arsenic;[6] with controlled (and fairly large) radii, these nanotubes can be made clean and without the problems of unknown chirality and intershell coupling that are present in multiwall carbon nanotubes (MWCNT).

II. THE ENERGY SPECTRUM

Since the effects we are to discuss resulting from the curvature are geometric rather than band-structure effects, and since the quantum Hall effect is formed in an inversion layer, we take as a model the above-mentioned inversion layer nanotubes. If x,y are the longitudinal and circumferential coordinates of the tube, respectively, the magnetic field B is perpendicular to the surface at the lines $y=0$ and $y=\pi R$, hereafter called the north and south ''poles .'' The ''equators'' are then at $y=\pi R/2$ and $y=3\pi R/2$, and states located anywhere above or below the equators are denoted ''north'' or '''south'' states. The effective vector potential on the surface of the tube has only the x component $A_x=RB\sin(y/R)$. The Hamiltonian of a cylindrical 2DEG is then

$$H=-\frac{\hbar^2\partial_y^2}{2m}+\frac{\hbar^2}{2m}\left(-i\partial_x+\frac{eRB}{\hbar}\sin\frac{y}{R}\right)^2+\mu g\mathbf{s}\cdot\mathbf{B}, \quad (1)$$

where g is the gyromagnetic factor (taken here at the value 2) and $\mathbf{s}$ is the spin operator. The longitudinal wave vector and spin are conserved since the Hamiltonian (1) does not contain the y coordinate nor other spin operators, thus the operators are replaced by their corresponding eigenvalues K_x and $\pm g\mu B/2$. In units of $E_R\equiv\hbar^2/2mR^2$ (which will be used throughout this work), Eq. (1) becomes the following one-dimensional Hamiltonian,

$$H=-R^2\partial_y^2+\left(K_xR+\eta\sin\frac{y}{R}\right)^2\pm\eta, \quad (2)$$

where, in addition $\eta\equiv(R/l)^2\gg1$ throughout this work. The Hamiltonian (2) is a variant of Hill's equation and can be easily diagonalized numerically.[3] The typical energy spectrum and probability distribution in this regime are shown in Fig. 1; the eigenfunctions are centered around their potential minima, depending on their longitudinal wave vector, K_x; these minima are at $y^n_{\min}=-R\sin^{-1}\alpha$ and $y^s_{\min}=\pi R-y^n_{\min}$, where the n and s subscripts stand for the ''north'' and ''south'' potential wells, and α is defined in the following way:

$$\alpha=\begin{cases}\dfrac{K_xR}{\eta} & \text{if} \quad -\dfrac{\eta}{R}<K_x<\dfrac{\eta}{R},\\ 1 & K_x\geqslant\dfrac{\eta}{R},\\ -1 & K_x\leqslant-\dfrac{\eta}{R}.\end{cases} \quad (3)$$

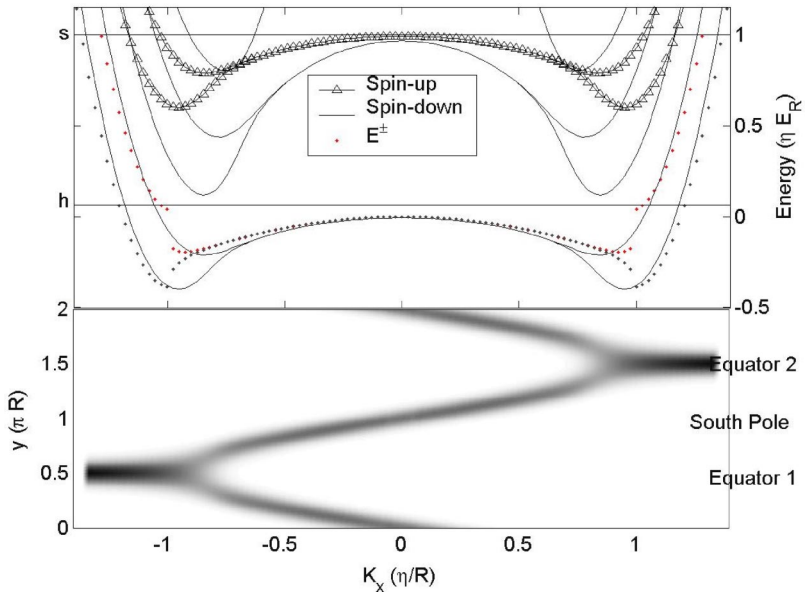

FIG. 1. Top: Energy spectrum of Eq. (2), calculated numerically for $\eta=20$. The lowest band is compared with the variational result, $E^{\pm}$, of Eq. (4). Bottom: Spatial probability distribution along the circumferential coordinate of the states at the lowest subband. Here the electrons are well confined to the proximity of their potential minima. At $K_x=0$ the potential in Eq. (2) is a double well, one at each pole. As $|K_x|$ increases, the two wells move closer towards one of the equators, and when $|K_x|\geqslant\eta/R$ they merge to one well, at the equator.

Since the Hamiltonian (2) is symmetric under a simultaneous sign inversion of y and K_x, states with opposite K_x are centered at opposite sides of the circumference, and states with $K_x=0$ are thus centered at the poles. At $|K_x|\ll\eta/R$ the potential has two deep and isolated potential wells in the north and south, giving rise to the twofold degeneracy of the spectrum. Only as $|K_x|\to\eta/R$ are the two potential wells at sufficient proximity across one of the equators for their corresponding states to mix and remove the degeneracy.

We can find an analytic approximation to the spectrum of the lowest band, by making an ansatz on the variational wave function, in accordance with the discussion above. Up to a normalization factor, let the circumferential eigenfunctions of a state K_x be $\psi_k^{\pm}(y)=\chi_k^n\pm\chi_k^s$, where χ_k^n,χ_k^s are the single-well harmonic solutions of the north and south potential wells, respectively. At the lowest band, we therefore guess $\chi_k^{n/s}=Ae^{-\eta(y-y_{\min}^{n/s}+\lambda_{n/s})^2/2R^2}$, where $y_{\min}^{n/s}$ is the north or south coordinate of the potential minima. As $|K_x|\to(\eta/R)_-$, the north-south splitting evolves into the two eigenstates of a single, highly anharmonic, potential well, at the equator. The variational parameter $\lambda_{n/s}$ accounts for that by keeping the two eigenfunctions slightly apart; the best fit was found at $\lambda_{n/s}=0$ if $|y^s-y^n|>l$ and $\mp l/2$ otherwise; the minus sign corresponds to the north for negative K_x and to the south for positive K_x.

The energy of the symmetric $(+)$ and antisymmetric $(-)$ subbands is then found by $E^{\pm}=\langle\chi_k^n|H\chi_k^n\rangle\pm\langle\chi_k^n|H\chi_k^s\rangle$. The result gives the following spectrum:

$$E^{\pm}C^{\pm}=(K_xR-\alpha\eta)^2+\eta(1-\alpha^2)+\tfrac{1}{2}K_xR\alpha\pm e^{-\eta\Delta^2/R^2}[(|K_x|R-\eta)^2-\tfrac{1}{2}|K_x|R], \quad (4)$$

where $C^{\pm}=\langle\psi_k^{\pm}|\psi_k^{\pm}\rangle=(1\pm e^{-\eta\Delta^2/R^2})$ and $\Delta=R[(\pi/4)-\frac{1}{2}\sin^{-1}|\alpha|+|\lambda|/R]$. The spin term was *omitted* from Eq. (4) and the subsequent equations to avoid confusion with the $\pm$ sign of the symmetric and antisymmetric subbands. It is understood, however, that the spin further splits the spectrum by $\pm\eta$. The spectrum of Eq. (4) approximates the exact solution in a satisfactory way apart from the vicinity of $|K_x|\approx\eta/R$, as shown in Fig. 1.

Simplified expressions can be obtained from Eq. (4) if $|\alpha|$ is not too close to 1. For states not centered on the equator ("bulk" states), $E\approx\eta\cos\alpha$ while $E^{\pm}\approx(|K_x|R-\eta)^2+D^{\pm}|K_x|R$ for equator states, where $D^{\pm}=(e\mp1)/[2(e\pm1)]\approx0.23$ and 1.08, respectively.

The energy of higher subbands can be similarly obtained analytically; here we need, however, only the energy of the pole states at those subbands; these are easily obtained by expanding the potential in Eq. (2) around $K_x=0$, giving the (spinless) Landau-like levels at the poles,

$$E_n^P=\eta(2n+1)-\frac{1}{2}\left(n^2+n+\frac{1}{2}\right), \quad (5)$$

where the first term is the usual Landau levels, and the second term is the anharmonic correction due to the curvature. The velocity associated with a state K_x can be found from the dispersion relation (4); the average velocity of the two subbands is given by $v_k=-(\hbar/2mR)\alpha$ for the bulk states and $v_k=(\hbar/mR)(K_xR-\eta)$ for the equator states.

In the flat 2DEG, the energy of a the nth Landau level of spin down, is degenerate with the $n-1$ level of spin up. Here, however, for the Landau-like levels at the poles, this degeneracy is removed due to the second term on the right-hand side of Eq. (5). By fixing the Fermi energy in this gap $(E_1^P-\eta<E_F<E_0^P+\eta)$, only spin-up states would cross the Fermi energy at the poles; using Eq. (5) this gives $2\eta-\frac{5}{4}<E_F<2\eta-\frac{1}{4}$; this energy window is due to our arbitrary choice of $g=2$ for the g factor in Eq. (1); in general, for $g=2c$ with c a constant, the corresponding filling energy is $\eta(3-c)-\frac{5}{4}<E_F<\eta(1+c)-\frac{1}{4}$. In this window of width 1 $(=E_R)$ we get the typical spin distribution of Fig. 2 (top). There are two counterpropagating spin-up currents at the poles; each current is the sum of two states, with a velocity $-(\hbar/2mR)\alpha$, as calculated above.

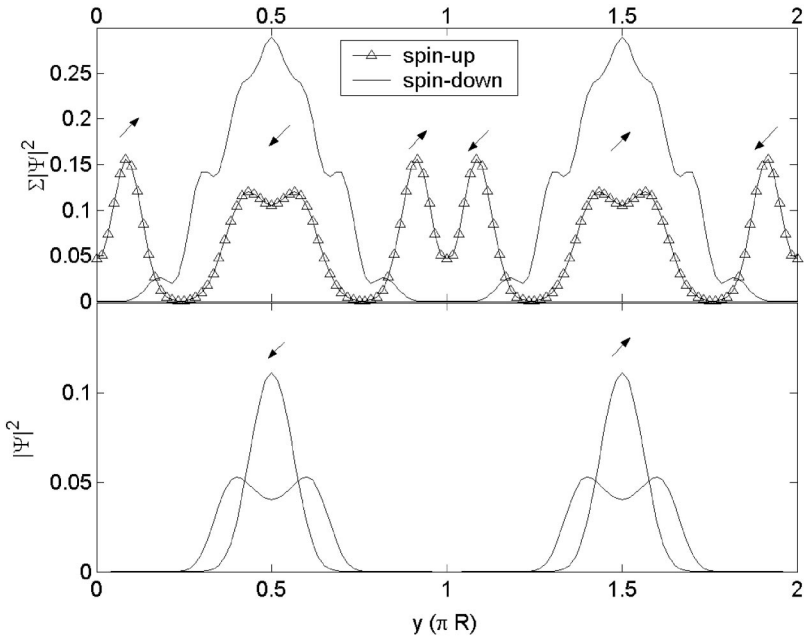

FIG. 2. The probability distribution of states at the Fermi energy. Top: The sum of all spin-up and spin-down states at the Fermi energy $E_F \lesssim \eta$ (line "s" in Fig. 1). There are a total of 20 states (ten channels). The arrows show the direction of propagation of these circumferentially localized states. Bottom: $E_F \gtrsim 0$ (line "h" in Fig. 1). At this energy there are only two equator states along each direction of propagation. The plotted probabilities correspond to $\eta=30$ and $\eta=50$ for the top and bottom figures, respectively (e.g., if 25 nm$\leqslant R \leqslant$100 nm, $\eta=30$ is achieved by the field 31.6 T$\geqslant B \geqslant$1.9 T, where the lower field corresponds to the larger radius).

III. LONGITUDINAL CONDUCTANCE

We wish to see next how the conductance is altered by the spatial redistribution of the wave functions. We show in the Appendix that the transmission of a state $\psi(y)$ in a tube located between two barriers, 1 and 2, is [Eq. (A2)] $T_{12}=\int dy\,|\psi(y)|^2(T_1T_2)/\{1+R_1+R_2-2\sqrt{R_1R_2}\cos[2\theta_B(y)+\theta]\}$, where $\theta_B(y)=(\eta/R)x\sin(y/R)$, θ is a constant, and R,T are the reflection and transmission probabilities of each barrier.

Using Eq. (A2) we can find the conductance of the Hall state, where the filling corresponds to line "h" in Fig. 1, i.e. where only the two equator channels are gapless. In that case, the total conductance of the two channels is found to be (see the Appendix)

$$\frac{\hbar}{e^2}G_{xx}=T_{12}=2T_{eq}-\left(\frac{T_{eq}}{T_1T_2}\right)^2\frac{\beta\sqrt{R_1R_2}\sin\left(2\eta\frac{L}{R}+\theta\right)}{\eta(1-e^{-1/4})}, \tag{6}$$

where L is the tube length, $\beta\equiv(\eta L/R)\mathrm{mod}(2\pi)$, and $T_{eq}\equiv(T_1T_2)/[1+R_1+R_2-2\sqrt{R_1R_2}\cos(2\eta L/R+\theta)]$. The first term, $2T_{eq}$, gives the transmission of two y-localized states at the equator, i.e., for $\psi(y)=\delta(y-y_{eq})$, it gives Aharonov-Bohm-like oscillations due to the flux enclosed by the equators, with a period of oscillations of $\Delta B=h/(2eRL)$. Similar oscillations were predicted[9] and observed[10] in a disk under a strong magnetic field; there, chiral edge states formed at the circumference oscillate with the enclosed flux. The second term in Eq. (6) contains the difference, since here, the lateral width of the wave function was not neglected, allowing for contribution from paths which are slightly off the equator, enclosing different fluxes; in the limit of infinite field ($\eta\to\infty$), this correction reduces to zero, as it should, since then the wave function becomes $\psi(y)\to\delta(y-y_{eq})$.

The magnetoconductance experiments conducted on large nanotubes (MWCNT),[4,5] were inconclusive and the subject of some debate (see Ref. 11). Since the total longitudinal conductance comes from all the subbands crossing the Fermi energy, it is clear that as the field varies, the number of open channels may abruptly change, adding an aperiodic, band-structure-dependent element to the magnetoconductance, as suggested in Ref. 5.

IV. HALL CONDUCTANCE

We focus below on the small window of energy filling (line "h" in Fig. 1) where the conductance is carried solely by the equator states, as shown in Fig. 2 (bottom); the reason is its topological equivalence to the Hall bar in the integer quantum Hall effect.[12] Here the Hall voltage can be defined as the potential drop between the equators.

Having found the longitudinal conductance [Eq. (6)], we wish to establish the quantization of Hall conductance and its range of validity, by applying some results from the extensive studies of the quantum Hall effect in the framework of the Landauer formalism.[9,13,16,17] In the simplest case, when scattering is absent, the current is $I=(Ne/h)(\mu_1-\mu_2)$, where μ_1,μ_2 are the chemical potentials of contacts 1 and 2, respectively, and N is the number of channels (two in our case). Since the equator (edge) currents are chiral, each equator is fed by a different contact, so that μ_1,μ_2 are the chemical potentials of equators 1 and 2, respectively, resulting in the quantized Hall conductance of $G_{xy}=Ne^2/h$ (where $N=2$ in our example, with the filling at line "h" in Fig. 1).

Let us now relate the number of equator channels to the actual electron density. The maximum density of "bulk" states, i.e., states with potential minima not at the equators, is the number of K_x states satisfying $|\alpha|<1$, divided by the area, giving $\max(n_{\mathrm{bulk}})=(L/2\pi)(2\eta/R)/(2\pi RL)$ per subband. Defining the tube filling as the filling fraction of the available "bulk" states, $\nu_{\mathrm{tube}}\equiv n_{\mathrm{bulk}}/\max(n_{\mathrm{bulk}})$

$=2\pi^2R^2n_{\rm bulk}/\eta$. When $n_{\rm bulk}\to n$ (see Ref. 14) and substituting $R^2/\eta=l^2$ we get

$$\nu_{\rm tube}=\pi\nu_{\rm bar}, \tag{7}$$

relating our filling to the conventional Hall bar $\nu_{\rm bar}$. In the case of a valley degeneracy, $\max(n_{\rm bulk})$ is multiplied by the number of valleys so that the actual $\nu_{\rm tube}$ in Eq. (7) must be divided by their number. In our example, however, with a single valley, the quantum Hall filling is at $\nu_{\rm tube}\gtrsim 2$.

Several problems may hinder this quantization, which we address next. First, it was shown experimentally that in narrow Hall bars the quantum Hall effect is quenched.[15] The quenching occurs whenever the lateral energy becomes comparable to the Landau level. This problem is avoided here, by definition, since we work in the $\eta\gg 1$ regime. A second problem is the effect of scattering. It was shown,[16] however, that the Hall conductance remains quantized even when scattering is included, given that a local equilibrium is established at the potential probes (i.e., the probes are at least an inelastic length away from the scatterers). In the absence of such an equilibrium, G_{xy} is not quantized and depends on G_{xx}. In the case of a two-terminal setup this dependence takes on a particularly elegant form[17] by the sum rule $(G_{xx}^{-1}+G_{xy}^{-1})^{-1}=(e^2/h){\rm Tr}(tt^+)$, where t is the scattering matrix. The oscillations we found in G_{xx} [Eq. (6)] translate in this case to small oscillations of G_{xy} around its quantized value.[9]

V. DISCUSSION

The currents discussed in this work are due to the high η field, which both localizes a state along the circumference, and, due to the strong gradients, bends the energy band in k space, according to the real-space location of its eigenstate. Accordingly, any curved 2DEG should generate spin currents, given $\eta\gg 1$ (where η of a general curved surface can be defined locally, if the radius of curvature, R, is constant over an arc length $\gg l$). A hemicylinder, for example, has the same physics as a cylinder in all but one feature: there is no north-south degeneracy nor is there north-south mixing, and hence, no subband splitting as in our spectrum; that point, however, had negligible effect on the spin-current distribution. The apparent advantage of a curved 2DEG over a nanotube is the possibility to attach the contacts lithographically to only a small region along the curved surface; this may allow to harness the spin currents for spintronics applications in an integrated solid-state device.

In conclusion, we showed that in strong fields, chiral spin currents propagate along the tube at different spatial locations with different velocities. We suggest the observation of this effect with a spin-polarized scanning-tunneling microscope;[8] the possibility to harness the spin currents for spintronics applications with a general curved 2DEG has already been pointed out. In a fully spin-polarized filling, the magnetoconductance G_{xx} has a periodic component, with a period of the flux enclosed by the equators. The Hall conductance is quantized if local equilibrium is established at the voltage probes; otherwise, it has small oscillations about its quantized value, which is $G_{xy}=2e^2/h$ around a filling $\nu_{\rm tube}\gtrsim 2$.

ACKNOWLEDGMENT

I am indebted to Sebastian Eggert for numerous helpful discussions.

APPENDIX: DERIVATION OF EQ. (6)

Below we derive a general expression for the conductance of a nanotube under a perpendicular field, and apply it to obtain explicitly the conductance of the lowest two equator channels. We assume a tube of length L lying between two barriers, 1 and 2, whose s matrices are given by

$$s_1=\begin{pmatrix} r_1 & t_1^* \\ t_1 & r_1^* \end{pmatrix}$$

and

$$s_2=\begin{pmatrix} r_2 & t_2^* \\ t_2 & r_2^* \end{pmatrix}.$$

Recall that the transmission amplitude of a single mode on a line between barriers 1 and 2 is $t_{line}=t_2t_1+t_2r_1^*r_2t_1+t_2r_1^*r_1^*r_2t_1+\cdots=(t_1t_2)/(1-r_1^*r_2)$. The transmission probability is then given by $T_{line}=|t_{line}|^2=(T_1T_2)/[1+R_1+R_2-2\sqrt{R_1R_2}\cos\theta]$ where $\theta=2\phi+{\rm phase}(r_1^*)+{\rm phase}(r_2^*)$, where ϕ is the ''optical'' phase. Here, in contrast to a line, both the amplitude and the phase are functions of the lateral coordinate y. The correct transmission amplitude of a single mode is then

$$t(y)=\psi_k(y)t_1e^{i\theta_B(y)}t_2+\psi_k(y)t_1e^{i\theta_B(y)}r_2^*e^{i\theta_B(y)}r_1e^{i\theta_B(y)}t_2+\cdots=\psi_k(y)e^{i\theta_B(y)}\frac{t_1t_2}{1-r_1^*r_2e^{i2\theta_B(y)}}, \tag{A1}$$

where $\psi_k(y)$ is the appropriate solution of Eq. (2), and $\theta_B(y)$ is the phase factor along x due to the field, $\theta_B(y)=(e/\hbar)A_xx=(eRB/\hbar)x\sin(y/R)=(\eta/R)x\sin(y/R)$; note that since right and left movers are located at opposite sides of the circumference, θ_B doesn't change sign as a particle backscatters at a barrier, since both $x\to -x$ and $y\to -y$. Now the total transmission is

$$T_{12}=\int dy\, t(y)t^*(y)=\int dy|\psi(y)|^2\frac{T_1T_2}{1+R_1+R_2-2\sqrt{R_1R_2}\cos[2\theta_B(y)+\theta]}. \tag{A2}$$

Equation (A2) gives the general expression for the transmission of a channel whose lateral state is given by $\psi(y)$.

As an application of Eq. (A2), let us calculate the transmission of the first two equator channels. The phase factor accumulated after propagating a distance L in the proximity

of an equator is $\theta_B(y,x=L)\approx(\eta L/R)\{1-[(y-y_{eq})^2/2R^2]\}$ where y_{eq} is the coordinate of one of the equators. Consequently, the cosine in the integrand in Eq. (A2) reads $\cos[2\theta_B(y,x=L)+\theta]\approx\cos[2\eta(L/R)+\theta]-\beta\sin[2\eta(L/R)+\theta][(y-y_{eq})/R]^2$, where $\beta\equiv(\eta L/R)\bmod(2\pi)$. Then, to second order in $(y-y_{eq})/R$, Eq. (A2) becomes

$$T_{12}=T_{eq}-\frac{2T_{eq}^2\beta\sqrt{R_1R_2}\sin\left(2\eta\frac{L}{R}+\theta\right)}{(T_1T_2R)^2}\int dy\,|\psi(y)|^2\times(y-y_{eq})^2, \tag{A3}$$

where $T_{eq}\equiv(T_1T_2)/\{1+R_1+R_2-2\sqrt{R_1R_2}\cos[2\eta(L/R)+\theta]\}$. We estimated $\psi(y)$ in connection with the variational calculation of the spectrum in Eq. (4). The lowest two equator states are given by

$$\psi^{\pm}=1/[2(1\pm e^{-1/8})]\sqrt{\eta/\pi R^2}\times[e^{-\eta(y-y_{eq}-R/\sqrt{\eta})^2/2R^2}\pm e^{-\eta(y-y_{eq}+R/\sqrt{\eta})^2/2R^2}],$$

where $\pm$ refers to the symmetric and antisymmetric states. The integral in Eq. (A3) then yields $R^2/[4\eta(1\pm e^{-1/8})]$. The combined conduction of the two equator channels, $T_{12}=T_{12}^{+}+T_{12}^{-}$, given by Eq. (A3) is then

$$T_{12}=2T_{eq}-\left(\frac{T_{eq}}{T_1T_2}\right)^2\frac{\beta\sqrt{R_1R_2}\sin\left(2\eta\frac{L}{R}+\theta\right)}{\eta(1-e^{-1/4})}, \tag{A4}$$

where the factor $1-e^{-1/4}$ comes from the choice of the variational wave function [see Fig. 1 and Eq. (4)], so it is of course only an approximate numerical factor.

[1] R. Saito, G. D. Dresselhaus, and M. S. Dresselhaus, *Physical Properties of Carbon Nanotubes* (Imperial College, London, 1998).

[2] G. Sallis, Y. Kato, K. Ensslin, D. C. Driscoll, A. C. Gossard, and D. D. Awschalom, Nature (London) **414**, 619 (2001).

[3] H. Ajiki and T. Ando, J. Phys. Soc. Jpn. **62**, 1255 (1993).

[4] C. Schönenberger, A. Bachtold, C. Strunk, J. P. Salvetat, and L. Forro, Appl. Phys. A: Mater. Sci. Process. **A69**, 283 (1999); C. Schönenberger and A. Bachtold, Phys. Rev. B **64**, 157401 (2001).

[5] J. O. Lee, J. R. Kim, J. J. Kim, J. Kim, N. Kim, J. W. Park, K. H. Yoo, K. H. Park, Phys. Rev. B **61**, R16 362 (2000); K. Kang, J. O. Lee, and J. J. Kim, *ibid.* **64**, 157402 (2001).

[6] V. Ya. Prinz, V. A. Seleznev, A. K. Gutakovsky, A. V. Chehovskiy, V. V. Preobrazhenskii, M. A. Putyato, and T. A. Gavrilova, Physica E (Amsterdam) **6**, 828 (2000).

[7] Oliver G. Schmidt and Karl Eberl, Nature (London) **410**, 168 (2001).

[8] S. Heinze, M. Bode, A. Kubetzka, O. Pietzsch, X. Nie, S. Blügel, and R. Wiesendanger, Science **288**, 1805 (2000).

[9] U. Sivan, Y. Imry, and C. Hartzstein, Phys. Rev. B **39**, 1242 (1989).

[10] B. J. van Wees, L. P. Kouwenhoven, C. J. P. M. Harmans, J. G. Williamson, C. E. Timmering, M. E. I. Broekaart, C. T. Foxon, and J. J. Harris, Phys. Rev. Lett. **62**, 2523 (1989).

[11] The magnetoconductance of MWCNT was found to oscillate aperiodically (Refs. 4 and 5). The former group assigned this to universal conductance fluctuations, which comes about in a diffusive 2D conductor, while the latter attributed the fluctuations to variations in the density of states. With $B\lesssim 10$ T and typical tube radii of 10 nm and 15 nm in Refs. 4 and 5, respectively, they had $\eta\lesssim 1.5$ and $\eta\lesssim 3.3$, at the lower edge of our regime.

[12] R. B. Laughlin, Phys. Rev. B **23**, 5632 (1981).

[13] J. K. Jain, Phys. Rev. Lett. **60**, 2074 (1988).

[14] In the Hall bar the density of bulk states $n_{\rm bulk}$, is normally equated with the total density n, so that the fraction of the edge states in the total density is neglected when the filling fraction ν is expressed in terms of density. Here we may do so on account of the divergency of the ''bulk'' density of states close at the poles. The equator density of states, on the other hand, does not diverge. Further, since at low filling the highest $|K_x|$ is only slightly larger than η/R, the part of the equator states in the total density can be neglected here as well.

[15] A. Scherer, S. J. Allen, Jr., H. G. Craighead, R. M. Ruthen, E. D. Beebe, and J. P. Harbison, Phys. Rev. Lett. **59**, 3011 (1987).

[16] M. Büttiker, Phys. Rev. B **38**, 9375 (1988).

[17] P. Streda, J. Kucera, and A. H. MacDonald, Phys. Rev. Lett. **59**, 1973 (1987).